Cite this article as: Narayan Sundaram and T.N.Farris: Mechanics of Advancing Pin-loaded Contacts with Friction. *Journal of the Mechanics and Physics of Solids.* **58**(2010) pp. 1819–1833. doi:10.1016/j.jmps.2010.08.004

Mechanics of Advancing Pin-loaded Contacts with Friction

Narayan Sundaram [a,*] T.N. Farris [b]

[a] *School of Aeronautics and Astronautics, Purdue University,701 W. Stadium Ave., West Lafayette, IN 47907-2045*

[b] *School of Engineering, Rutgers, The State University of New Jersey, 98 Brett Rd., Piscataway, NJ 08854-8058*

Abstract

This paper considers finite friction contact problems involving an elastic pin and an infinite elastic plate with a circular hole. Using a suitable class of Green's functions, the singular integral equations governing a very general class of conforming contact problems are formulated. In particular, remote plate stresses, pin loads, moments and distributed loading of the pin by conservative body forces are considered. Numerical solutions are presented for different partial-slip load cases. In monotonic loading, the dependence of the tractions on the coefficient of friction is strongest when the contact is highly conforming. For less conforming contacts, the tractions are insensitive to an increase in the value of the friction coefficient above a certain threshold. The contact size and peak pressure in monotonic loading are only weakly dependent on the pin load distribution, with center loads leading to slightly higher peak pressure and lower peak shear than distributed loads. In contrast to half-plane cylinder fretting contacts, fretting behavior is quite different depending on whether or not the pin is allowed to rotate freely. If pin rotation is disallowed, the fretting tractions resemble half-plane fretting tractions in the weakly conforming regime but the contact resists sliding in the strongly conforming regime. If pin rotation is allowed, the shear traction behavior resembles planar rolling contacts in that one slip zone is dominant and the peak shear occurs at its edge. In this case, the effects of material dissimilarity in the strongly conforming regime are only secondary and the contact never goes into sliding. Fretting tractions in the forward and reversed load states show shape asymmetry, which persists with continued load cycling. Finally, the governing integro-differential equation for full sliding is derived; in the limiting case of no friction, the same equation governs contacts with center-loading and uniform body-force loading, resulting in identical pressures when their resultants are equal.

1 Introduction

The problem of contact between geometrically conforming surfaces is important in many contexts. The analysis of such contacts is complicated by the fact that the half-plane assumption used in the classical Hertzian formulation is invalid. While frictionless conforming contact systems have been investigated in the past in both the advancing and receding regimes (see Gladwell (1980)), partial slip behavior of conforming contacts remains relatively unexplored. Prior work in this area has consisted of FEA (Iyer, 2001), the use of simplified contact models (Ho and Chau, 1997) and an approximate treatment of similar contacts by modeling the clearance as a slit in a continuum (Hou and Hills, 2001).

The use of Green's functions representing point- normal and tangential boundary loading of an elastic domain usually provides a very flexible means of formulating contact problems involving that domain; in particular, there are no symmetry or smoothness requirements of the unknown tractions and no restrictions on the extent of 'mixity' of the boundary conditions. Despite this, it may be noted that the closed form of the Green's functions have rarely been used to model conforming contact problems; for instance, recent work on frictionless contact formulation (To et al., 2007) relies on the use of infinite series. The factors complicating such a first-principles formulation are the lack of ready availability of the counterparts of Flamant's half-plane potentials for the pin and analytical difficulties introduced by the circular geometry. The latter may (as it will be seen) be overcome by the introduction of a suitable linear differential operator and the use of a generalized function framework.

The objective of this work is to provide an exact formulation of the equations governing advancing conforming contact systems in partial slip (and sliding); the resulting equations are subsequently solved numerically. Recent work by the authors (Sundaram and Farris, 2010) considered the analytically simpler case of a rigid pin. The present work treats the case when the pin/disk is deformable and elastically dissimilar to the infinite plate, with the applied loads possibly acting as body forces on the pin. Modeling body forces is appealing in that one avoids the singular stresses that occur with center loading.

Of course, in applications, the distribution of loads on the pin is likely to be of quite complicated form (unless one considers simple cases like a pin pushed against a cradle by its own weight) and its exact specification difficult. In addition, the transmission of loads along the length of pinned connections has a definite three dimensional aspect to it and this raises the problem of converting the shear stress in any section into a specific body force distribution on a cross section of the pin in a two-dimensional analysis. Even more, such a distribution would be application dependent and its

* Corresponding author.
Email addresses: nsundara@purdue.edu (Narayan Sundaram), tfarris@rutgers.edu (T.N. Farris).

generality questionable. Rather than attempt this, one may instead consider uniform body force loading and center loading as two extreme types of load distributions on the pin, with realistic equivalent loading of the pin lying in-between. If (as it will be seen) the distribution of loads on the pin does not drastically alter the nature of the tractions, one may consider these as providing bounds for tractions likely to be seen under more general loading conditions.

This paper is organized as follows. Fundamental solutions for the pin, plate and the surface displacements caused by them are summarized in section 2. These displacements are subsequently used in section 3 to formulate the equations governing partial slip contact. In section 4, the formulation is adapted to accommodate body-force loading of the pin. In section 5, numerical solutions to various types of partial slip problems are presented for both similar and dissimilar contacts. Differences with half-plane fretting behavior and some special cases are discussed in section 6.

2 Green's functions and surface displacements

Point loads of the type shown in Fig. 1(a) are sufficient to represent the most general tractive state of a center-loaded pin with appropriate use of superposition and rotation. Problem I consists of a normal load $-N$ applied at $\theta = 0$ on the boundary point $z = a$ with an equal and opposite load N applied at the center of the pin $z = 0$. Problem II consists of a tangential point load T applied at the point $z = a$ and an equal and opposite point load $-T$ acting at the center, with an additional moment M to offset the resulting couple at the center of the pin.

Both problems may be solved by the use of standard complex variable techniques, as described in England (1971) or Muskhelishvili (1954). For a pin centered at the origin, the Kolosov-Muskhelishvili potentials for problem (I) are given by

$$\Omega(z) = -c\log(z) + c(1+\kappa_I)\log(z-a) + \frac{c(1+\kappa_I)}{2a}z + \frac{c}{a^2}z^2 \tag{1}$$

$$\omega(z) = \kappa_I c\log(z) - c(1+\kappa_I)\log\left(1-\frac{z}{a}\right) - c(1+\kappa_I)\frac{a}{z-a} \tag{2}$$

Where a is the radius of the pin, κ_I its Kolosov's constant and $c = N/2\pi(1+\kappa_I)$. For problem (II), one has

$$\Omega(z) = ic\log(z) - ic(1+\kappa_I)\log(z-a) + \frac{ic}{a^2}z^2 + \frac{iM}{2\pi a^2}z \tag{3}$$

$$\omega(z) = i\kappa_I c\log(z) - ic(1+\kappa_I)\log\left(1-\frac{z}{a}\right) + ic(1+\kappa_I)\frac{a}{z-a} + \frac{iM}{2\pi}\frac{1}{z} \tag{4}$$

where $M = -Ta$ and $c = T/2\pi(1+\kappa_I)$.

One is concerned only with *surface* displacements in a contact formulation; these are

easily derived from the Kolosov-Muskhelishvili potentials Eqs. (1)-(4). Introduce the function

$$A(\theta) = \frac{\theta + \pi}{2} - \pi H(\theta) = \frac{\theta}{2} - \frac{\pi}{2}\,\mathrm{sign}(\theta) \tag{5}$$

The surface displacements for problem (I) are then given by

$$2G_I(\tilde{u}_r + i\tilde{u}_\theta) = \frac{N}{2\pi}\left\{e^{i\theta} + \frac{\kappa_I + 1}{2}\left[1 + e^{-i\theta}\log(2 - 2\cos\theta)\right] + ie^{-i\theta}(\kappa_I - 1)A(\theta)\right\} \tag{6}$$

When the normal load N acts at an arbitrary point $z = ae^{i\xi}$ on the boundary of the pin rather than $z = a$ (with the load at the origin rotated correspondingly to maintain equilibrium), the displacements are obtained simply by replacing θ by $\theta - \xi$. Introduce the notation

$$A \equiv A(\theta,\xi) \equiv \frac{\theta - \xi}{2} - \frac{\pi}{2}\,\mathrm{sign}(\theta - \xi) \qquad C \equiv C(\theta,\xi) \equiv \cos(\theta - \xi) \tag{7}$$

$$L \equiv L(\theta,\xi) \equiv \log(2 - 2\cos(\theta - \xi)) \qquad S \equiv S(\theta,\xi) \equiv \sin(\theta - \xi) \tag{8}$$

Then, after separating real and imaginary parts, the surface displacements are

$$\left\{\tilde{u}_r^N \quad \tilde{u}_\theta^N\right\} = \frac{N}{4\pi G_I}\left\{C + \kappa_I^{'}\left[1 + CL\right] + \kappa_I^{''}SA \qquad S - \kappa_I^{'}SL + \kappa_I^{''}CA\right\} \tag{9}$$

where $\kappa_I^{'} = (\kappa_I + 1)/2$, $\kappa_I^{''} = (\kappa_I - 1)$. The superscript N denotes an applied normal load, and the subscript I denotes the pin's material properties.

For problem (II), the surface displacements are

$$\left\{\tilde{u}_r^T \quad \tilde{u}_\theta^T\right\} = \frac{T}{4\pi G_I}\left\{-S - \kappa_I^{'}SL + \kappa_I^{''}CA \qquad C - \kappa_I^{'}CL - \kappa_I^{''}SA\right\} \tag{10}$$

Kolosov-Muskhelishvili potentials for problems analogous to (I) and (II) for the plate were obtained by Rothman (1950). These may then be used to derive surface displacements (Sundaram and Farris, 2010). For ease of contact formulation, the positive directions for the loads on the pin and plate are chosen to be opposite to each other (i.e., T is clockwise positive on the plate). For a point normal load N acting at a boundary point $z = ae^{i\xi}$, the plate surface displacements (denoted by the letter v) are given by

$$\left\{\tilde{v}_r^N \quad \tilde{v}_\theta^N\right\} = \frac{N}{4\pi G}\left\{\kappa^{''}SA - \kappa^{'}CL \qquad \kappa^{'}SL + \kappa^{''}CA\right\} \tag{11}$$

where the elastic properties of the plate are given by the pair G, κ and $\kappa^{'} = (\kappa + 1)/2$, $\kappa^{''} = (\kappa - 1)$. When a tangential point load T (clockwise positive) acts at a point on the edge of the hole,

$$\left\{\tilde{v}_r^T \quad \tilde{v}_\theta^T\right\} = \frac{T}{4\pi G}\left\{\kappa^{''}CA + \kappa^{'}SL \qquad \kappa^{'}CL - \kappa^{''}SA\right\} \tag{12}$$

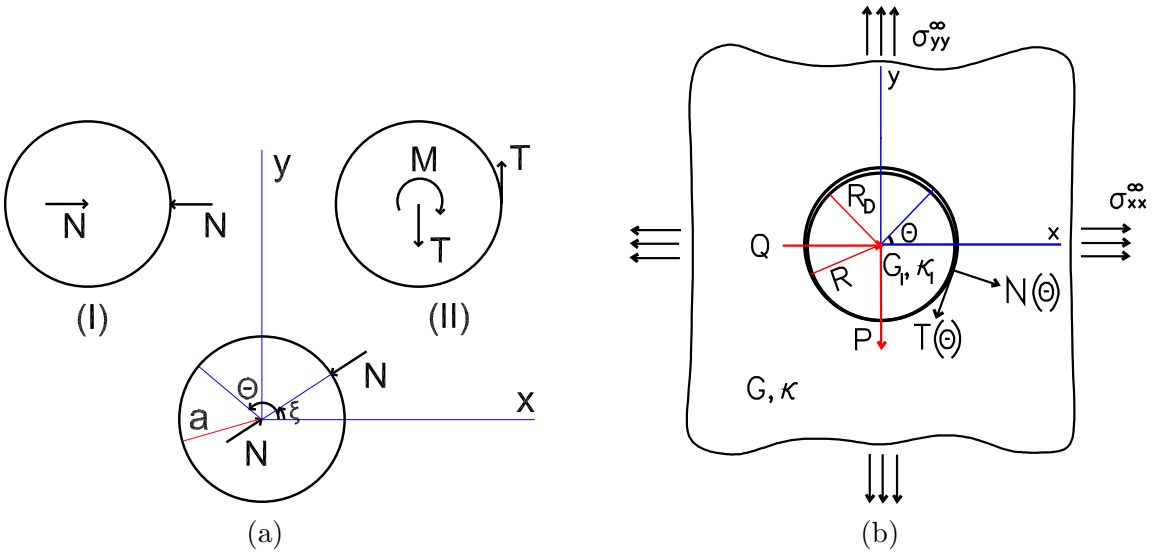

Fig. 1. Green's functions for the pin (left) and Conforming contact geometry(right)

3 Contact formulation

Let R_D and R be, respectively, the radii of the pin and the hole, where $R_D < R$. In the undeformed configuration, the pin rests on the plate as shown in Fig. 1(b). In this state, the reference gap function, $h_0(\theta)$, is

$$h_0(\theta) = (R - R_D)(1 + \sin(\theta)) \tag{13}$$

If the pin is now rotated by a small amount C_ω, and pressed into the elastic space by a rigid-body displacement vector $\overline{V} = (C_{0x}, -\Delta)$, the new gap function, $h_d(\theta)$ is

$$h_d(\theta) = (R - R_D)(1 + \sin(\theta)) - C_{0x}\cos(\theta) + \Delta\sin(\theta) \tag{14}$$

Note that the gap function is not affected by the rotation. The motion $\overline{V}$ causes overclosures; inside the contact, these overclosures must be relieved by elastic displacements in the pin and the plate. By definition, the gap function is

$$h(\theta) = h_d(\theta) + \tilde{v}_r - \tilde{u}_r = h_d(\theta) + \tilde{v}_r^{p,q} - \tilde{u}_r^{p,q} + \tilde{v}_r^{\infty} \tag{15}$$

where $\tilde{u}_r^{p,q}$ are the radial surface displacements of the pin due to the pressure and shear tractions, and $\tilde{v}_r^{p,q}$ the corresponding terms for the plate, and $\tilde{v}_r^{\infty}$ the contribution from the remote loads. One also has $h(\theta) = 0$ for all points in contact, so that

$$h_d(\theta) = (R-R_D)(1+\sin(\theta)) - C_{0x}\cos(\theta) + \Delta\sin(\theta) = -\tilde{v}_r^{p,q} + \tilde{u}_r^{p,q} - \tilde{v}_r^{\infty} \quad \forall\theta \in L \tag{16}$$

In partial slip problems, different considerations apply depending on whether or not the pin is allowed to rotate freely. For free rotation, *after* contact is established, the rotation of the pin is resisted by friction. For constrained rotation, the constraint generates a moment at the center of the pin. Including a rotation degree of freedom C_ω in the formulation with a corresponding moment in the global equilibrium equations allows both to be considered as special cases. The slip function $s(\theta)$, defined as the difference in tangential surface displacements of the pin and the plate in the presence of rotation is then [1]

$$s(\theta) = \tilde{u}_\theta^{rigid} + \tilde{u}_\theta - \tilde{v}_\theta \tag{17}$$
$$= C_\omega R - \Delta\cos(\theta) - C_{0x}\sin(\theta) + \tilde{u}_\theta^{p,q} - \tilde{v}_\theta^{p,q} - \tilde{v}_\theta^{\infty} \tag{18}$$

where $\tilde{u}_\theta^{p,q}$ are the tangential surface displacements of the pin due to tractions, and $\tilde{v}_\theta^{p,q}$ the corresponding terms for the plate. The terms containing Δ and C_{0x} are the tangential components of the rigid-body motion $\overline{V} = (C_{0x}, -\Delta)$ projected along the edge of the hole. The gap Eq. (16) and slip Eq. (18) inside the contact may be re-arranged as follows

$$\tilde{v}_r^{p,q} - \tilde{u}_r^{p,q} = (R_D - R)(1 + \sin(\theta)) + C_{0x}\cos(\theta) - \Delta\sin(\theta) - \tilde{v}_r^{\infty} \tag{19}$$
$$\tilde{v}_\theta^{p,q} - \tilde{u}_\theta^{p,q} = -s(\theta) - \Delta\cos(\theta) - C_{0x}\sin(\theta) - \tilde{v}_\theta^{\infty} + C_\omega R \tag{20}$$

Introduce the new variables

$$\tilde{X}_\theta^p = \tilde{v}_\theta^p - \tilde{u}_\theta^p \qquad \tilde{X}_\theta^q = \tilde{v}_\theta^q - \tilde{u}_\theta^q \tag{21}$$
$$\tilde{X}_r^p = \tilde{v}_r^p - \tilde{u}_r^p \qquad \tilde{X}_r^q = \tilde{v}_r^q - \tilde{u}_r^q \tag{22}$$

and define the matrix

$$\{\mathbb{M}\} = \left\{ \tilde{X}_r^p + \tilde{X}_r^q \qquad \tilde{X}_\theta^p + \tilde{X}_\theta^q \right\}^{Tr} \tag{23}$$

i.e.,

$$\{\mathbb{M}\} = \begin{Bmatrix} (R_D - R)(1 + \sin(\theta)) + C_{0x}\cos(\theta) - \Delta\sin(\theta) - \tilde{v}_r^{\infty} \\ -s(\theta) - \Delta\cos(\theta) - C_{0x}\sin(\theta) - \tilde{v}_\theta^{\infty} + C_\omega R \end{Bmatrix} \tag{24}$$

Introduce a linear differential operator $[\boldsymbol{\partial}]$ defined as follows

$$[\boldsymbol{\partial}] = \begin{bmatrix} 1 & \dfrac{\partial}{\partial\theta} \\ -\dfrac{\partial}{\partial\theta} & 1 \end{bmatrix} \tag{25}$$

Considering [2] that $R_D \approx R$, and expressing the displacements caused by the tractions

[1] A discussion on the role of rotation appears in a later section.
[2] The boundary conditions are applied to the deformed configuration in this instance.

in Eq. (23) as superpositions of displacements caused by point loads,

$$\{\mathbb{M}\} = R \begin{Bmatrix} \int_\alpha^\beta \left(\tilde{v}_r^N - \tilde{u}_r^N\right) d\xi + \int_\alpha^\beta \left(\tilde{v}_r^T - \tilde{u}_r^T\right) d\xi \\ \int_\alpha^\beta \left(\tilde{v}_\theta^N - \tilde{u}_\theta^N\right) d\xi + \int_\alpha^\beta \left(\tilde{v}_\theta^T - \tilde{u}_\theta^T\right) d\xi \end{Bmatrix} \tag{26}$$

where, of course, $N = N(\xi)$ and $T = T(\xi)$. Defining additional terms like $X_r^N = \tilde{v}_r^N - \tilde{u}_r^N$, and operating with $[\boldsymbol{\partial}]$,

$$[\boldsymbol{\partial}]\{\mathbb{M}\} = R \begin{Bmatrix} \int_\alpha^\beta X_r^N d\xi + \int_\alpha^\beta X_r^T d\xi + \frac{\partial}{\partial\theta}\int_\alpha^\beta X_\theta^N d\xi + \frac{\partial}{\partial\theta}\int_\alpha^\beta X_\theta^T d\xi \\ -\frac{\partial}{\partial\theta}\int_\alpha^\beta X_r^N d\xi - \frac{\partial}{\partial\theta}\int_\alpha^\beta X_r^T d\xi + \int_\alpha^\beta X_\theta^N d\xi + \int_\alpha^\beta X_\theta^T d\xi \end{Bmatrix} \tag{27}$$

If one allows derivatives in the sense of distributions, the manipulations become much easier because it is possible to interchange the order of integration and differentiation, i.e.

$$[\boldsymbol{\partial}]\{\mathbb{M}\} = R \begin{Bmatrix} \int_\alpha^\beta X_r^N d\xi + \int_\alpha^\beta X_r^T d\xi + \int_\alpha^\beta \frac{\partial}{\partial\theta} X_\theta^N d\xi + \int_\alpha^\beta \frac{\partial}{\partial\theta} X_\theta^T d\xi \\ -\int_\alpha^\beta \frac{\partial}{\partial\theta} X_r^N d\xi - \int_\alpha^\beta \frac{\partial}{\partial\theta} X_r^T d\xi + \int_\alpha^\beta X_\theta^N d\xi + \int_\alpha^\beta X_\theta^T d\xi \end{Bmatrix} \tag{28}$$

or

$$[\boldsymbol{\partial}]\{\mathbb{M}\} = R \begin{Bmatrix} \int_\alpha^\beta \left(X_r^{N,T} + \frac{\partial}{\partial\theta} X_\theta^{N,T}\right) d\xi \\ \int_\alpha^\beta \left(X_\theta^{N,T} - \frac{\partial}{\partial\theta} X_r^{N,T}\right) d\xi \end{Bmatrix} \tag{29}$$

where $X_r^{N,T} = X_r^N + X_r^T$ etc. From the displacement Eqs. (9)-(12), one finds

$$X_r^{N,T} = \frac{T}{4\pi}\left[\alpha^* CA + \beta^* SL + \frac{S}{G_I}\right] + \frac{N}{4\pi}\left[\alpha^* SA - \beta^* CL - \frac{C}{G_I} - \frac{\kappa_I + 1}{2G_I}\right] \tag{30}$$

$$X_\theta^{N,T} = \frac{N}{4\pi}\left[\beta^* SL + \alpha^* CA - \frac{S}{G_I}\right] + \frac{T}{4\pi}\left[\beta^* CL - \alpha^* SA - \frac{C}{G_I}\right] \tag{31}$$

where the composite material properties α^*, β^* are defined as

$$\alpha^* = \frac{\kappa - 1}{G} - \frac{\kappa_I - 1}{G_I} \qquad \beta^* = \frac{\kappa + 1}{2G} + \frac{\kappa_I + 1}{2G_I} \tag{32}$$

Also, considering the derivatives of the functions SA, SL, CA and CL with respect to θ

$$\frac{\partial}{\partial\theta}[SA] = S\left[\frac{1}{2} - \pi\delta(\theta - \xi)\right] + CA \qquad \frac{\partial}{\partial\theta}[SL] = CL + 1 + C \tag{33}$$

$$\frac{\partial}{\partial\theta}[CA] = C\left[\frac{1}{2} - \pi\delta(\theta - \xi)\right] - SA \qquad \frac{\partial}{\partial\theta}[CL] = \cot\left(\frac{\theta - \xi}{2}\right) - SL - S \tag{34}$$

so that

$$\frac{\partial}{\partial\theta}\left[X_r^{N,T}\right] = \frac{N}{4\pi}\left[\alpha^* CA + \alpha^* SA' - \beta^*\left(-SL - S + \cot\left(\frac{\theta-\xi}{2}\right)\right) + \frac{S}{G_I}\right] + \frac{T}{4\pi}\left[-\alpha^* SA + \alpha^* CA' + \beta^*\left(CL + 1 + C\right) + \frac{C}{G_I}\right] \quad (35)$$

where $A' = 1/2 - \pi\delta(\theta - \xi)$ in terms of the Delta function. Similarly,

$$\frac{\partial}{\partial\theta}\left[X_\theta^{N,T}\right] = \frac{N}{4\pi}\left[\beta^*\left(CL + 1 + C\right) + \alpha^*(CA' - SA) - \frac{C}{G_I}\right] + \frac{T}{4\pi}\left[\beta^*\left(-SL - S + \cot\left(\frac{\theta-\xi}{2}\right)\right) - \alpha^*(CA + SA') + \frac{S}{G_I}\right] \quad (36)$$

Using Eqs. (30), (31), (35) and (36) in Eq. (29), the intractable logarithmic terms are eliminated and the integrands simplify to

$$X_r^{N,T} + \frac{\partial}{\partial\theta}X_\theta^{N,T} = \frac{N}{4\pi}\left[\gamma C + \frac{\kappa+1}{2G} - \pi\alpha^*\delta(\theta-\xi)C\right] + \frac{T}{4\pi}\left[-\gamma S + \beta^*\cot\left(\frac{\theta-\xi}{2}\right) + \pi\alpha^*\delta(\theta-\xi)S\right] \quad (37)$$

$$X_\theta^{N,T} - \frac{\partial}{\partial\theta}X_r^{N,T} = \frac{N}{4\pi}\left[-\gamma' S + \beta^*\cot\left(\frac{\theta-\xi}{2}\right) + \pi\alpha^*\delta(\theta-\xi)S\right] + \frac{T}{4\pi}\left[-\gamma' C - \beta^* + \pi\alpha^*\delta(\theta-\xi)C\right] \quad (38)$$

where the additional interface material constants γ, γ' are defined as

$$\gamma = \beta^* + \frac{\alpha^*}{2} - \frac{2}{G_I} \qquad \gamma' = \beta^* + \frac{\alpha^*}{2} + \frac{2}{G_I} \quad (39)$$

Now, for continuous functions F with support $[\alpha, \beta]$ one has [3]

$$\int_\alpha^\beta F(\xi)C(\theta,\xi)\delta(\theta-\xi)d\xi = F(\theta) \qquad \int_\alpha^\beta F(\xi)S(\theta,\xi)\delta(\theta-\xi)d\xi = 0 \quad (40)$$

So that substituting the integrands from Eqs. (37),(38) in Eq. (29)

$$[\boldsymbol{\partial}]\{\mathbb{M}\} = \frac{R}{4\pi} * \begin{Bmatrix} \beta^*\int_\alpha^\beta \cot\left(\frac{\theta-\xi}{2}\right)T(\xi)d\xi - \pi\alpha^* N(\theta) - \gamma\int_\alpha^\beta ST(\xi)d\xi + \frac{\kappa'}{G}\int_\alpha^\beta N(\xi)d\xi + \gamma\int_\alpha^\beta CN(\xi)d\xi \\ \beta^*\int_\alpha^\beta \cot\left(\frac{\theta-\xi}{2}\right)N(\xi)d\xi - \beta^*\int_\alpha^\beta T(\xi)d\xi - \gamma'\int_\alpha^\beta CT(\xi)d\xi + \pi\alpha^* T(\theta) - \gamma'\int_\alpha^\beta SN(\xi)d\xi \end{Bmatrix} \quad (41)$$

[3] These follow from the definition of the Delta function

Next, let the $[\boldsymbol{\partial}]$ operator be applied to $\mathbb{M}$ as defined in Eq. (24). Now, the surface displacements caused by remote stresses acting on the plate are

$$\left\{\tilde{v}_r^{\infty} \quad \tilde{v}_\theta^{\infty}\right\} = \frac{R\kappa^{'}}{2G}\left\{\frac{\mathscr{A}}{2} + \mathscr{D}\cos(2\theta) \qquad -\mathscr{D}\sin(2\theta)\right\} \tag{42}$$

where $\mathscr{A} = \sigma_{xx}^{\infty} + \sigma_{yy}^{\infty}$, $\mathscr{D} = \sigma_{xx}^{\infty} - \sigma_{yy}^{\infty}$, $\kappa^{'} = (\kappa+1)/2$ so that

$$[\boldsymbol{\partial}]\{\mathbb{M}\} = \begin{Bmatrix} (R_D - R)(1+\sin(\theta)) - s'(\theta) - G_s(\theta) \\ C_\omega R - s(\theta) + (R - R_D)\cos(\theta) - G_p(\theta) \end{Bmatrix} \tag{43}$$

i.e., the use of $\boldsymbol{\partial}$ eliminates the approaches. The remote stress dependent functions $G_p(\theta)$ and $G_s(\theta)$ are defined as

$$\tilde{v}_r^{\infty} + \tilde{v}_\theta^{'\infty} \equiv G_s(\theta) = \frac{R\kappa^{'}}{2G}\left[\frac{\mathscr{A}}{2} - \mathscr{D}\cos(2\theta)\right] \tag{44}$$

$$\tilde{v}_\theta^{\infty} - \tilde{v}_r^{'\infty} \equiv G_p(\theta) = \frac{R\kappa^{'}}{2G}\mathscr{D}\sin(2\theta) \tag{45}$$

Finally, equating the expressions for $[\boldsymbol{\partial}]\{\mathbb{M}\}$ from Eqs. (41) and (43), the following system of coupled SIEs governing partial slip is obtained

$$\begin{aligned}(R_D - R)(1+\sin(\theta)) - s'(\theta) - G_s(\theta) = \frac{R}{4\pi}\Bigg[\beta^* \int_\alpha^\beta \cot\left(\frac{\theta-\xi}{2}\right) T(\xi)d\xi - \pi\alpha^* N(\theta) \\ -\gamma\int_\alpha^\beta \sin(\theta-\xi)T(\xi)d\xi + \frac{\kappa^{'}}{G}\int_\alpha^\beta N(\xi)d\xi + \gamma\int_\alpha^\beta \cos(\theta-\xi)N(\xi)d\xi\Bigg]\end{aligned} \tag{46}$$

$$\begin{aligned}C_\omega R - s(\theta) + (R - R_D)\cos(\theta) - G_p(\theta) = \frac{R}{4\pi}\Bigg[-\beta^*\int_\alpha^\beta T(\xi)d\xi - \gamma'\int_\alpha^\beta \cos(\theta-\xi)T(\xi)d\xi \\ +\pi\alpha^* T(\theta) + \beta^*\int_\alpha^\beta \cot\left(\frac{\theta-\xi}{2}\right)N(\xi)d\xi - \gamma'\int_\alpha^\beta \sin(\theta-\xi)N(\xi)d\xi\Bigg]\end{aligned} \tag{47}$$

It may be noted that the appearance of the slip function in pressure SIE (47) makes the system implicit. Further, if the contact is divided into zones of stick and slip, then

$$s(\theta) = s(\theta)_{prev} \qquad\qquad s'(\theta) = s'(\theta)_{prev} \quad \forall\theta \in stick \tag{48}$$

In the slip zones, Coulomb's law applied locally gives the magnitude of the shear tractions

$$T(\theta) = -\operatorname{sign}(s(\theta) - s(\theta)_{prev})\mu N(\theta) \quad \forall\theta \in slip \tag{49}$$

The following equations, representing global equilibrium of the tractions with the applied loads P, Q, must also be satisfied

$$\int_\alpha^\beta (T(\theta)\cos\theta - N(\theta)\sin\theta)\, d\theta = \frac{P}{R} \qquad \int_\alpha^\beta (T(\theta)\sin\theta + N(\theta)\cos\theta)\, d\theta = \frac{Q}{R} \tag{50}$$

with an additional equation to be satisfied depending on the treatment of rotation

$$C_\omega = 0 \quad \text{OR} \quad \int_\alpha^\beta T(\theta) d\theta = 0 \quad \text{OR} \quad \int_\alpha^\beta T(\theta) d\theta = -\frac{M}{R^2} \tag{51}$$

4 Contact formulation with body force loading

In what follows, it will be assumed that the body forces are conservative in nature, and that they act uniformly over the interior of the pin. The fundamental problem for body forces analogous to problem (I) consists of a point normal load $-N$ applied to the edge of the pin, balanced by uniform body forces of density $\mathscr{C}$ in the interior of the pin. This will be designated as problem (III). To re-use as much of the derivation from section 3 as possible and save tedious algebra, it is better to express this as the superposition of problem (I) and another problem (designated IIIa) in which the boundary is traction free, and a central point force $-N$ is balanced by body forces of the same density $\mathscr{C}$ (see Fig. 2). Again, using standard techniques, it is not difficult to show that the following Kolosov-Muskhelishvili potentials solve IIIa

$$\Omega(z) = -c\log z + \frac{c}{a^2}z^2 + \frac{\lambda_I + G_I}{4(\lambda_I + 2G_I)}\mathscr{C}z^2 \tag{52}$$

$$\omega(z) = \kappa_I c \log z \tag{53}$$

where $c = -N/(2\pi(1+\kappa_I))$, $\mathscr{C} = N/(\pi a^2)$ and λ_I is Lame's first constant for the pin. The surface displacements for this problem have a particularly simple form, given by

$$\left\{\tilde{u}_r^{B,N} \quad \tilde{u}_\theta^{B,N}\right\} = \frac{N}{4\pi G_I}\left\{-\tfrac{1}{2}\cos(\theta) \qquad -\tfrac{1}{2}\sin(\theta)\right\} \tag{54}$$

Note that the interior singularities in problem (IIIa) and (I) cancel each other. In a similar way, one may define fundamental problem (IV) as a superposition of problem (II) and another problem (IVa), in which a vertical load $+T$, acting at the center of the pin, is offset by distributed body forces with resultant $-T$. The displacements for problem (IVa) differ from those of (IIIa) only by a rotation of $\pi/2$, i.e.

$$\left\{\tilde{u}_r^{B,T} \quad \tilde{u}_\theta^{B,T}\right\} = \frac{T}{4\pi G_I}\left\{\tfrac{1}{2}\sin(\theta) \qquad -\tfrac{1}{2}\cos(\theta)\right\} \tag{55}$$

In this case, the singularity caused by the center-load $-T$ in problem (II) is canceled while that caused by the moment $M = -Ta$ remains. However, the resulting

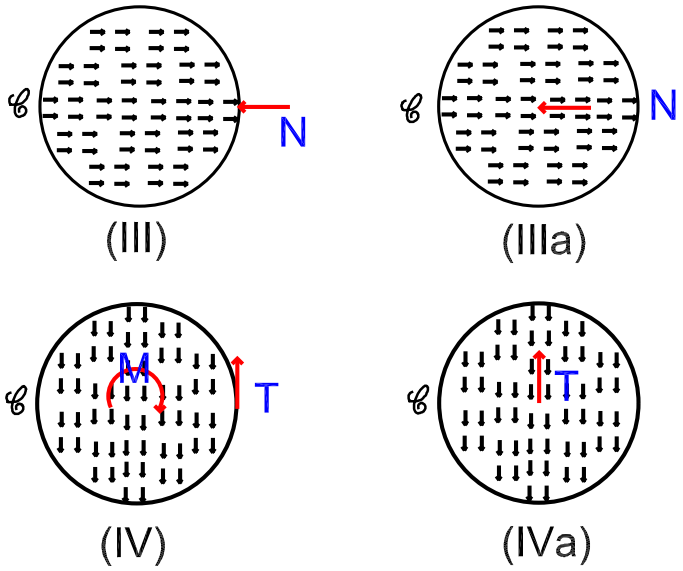

Fig. 2. Fundamental body force problems for the disk

distributed solution has no moment related singularity at the center of the pin (and consequently represents pure body force loading of the pin) if the shear is an odd function or free rotation of the pin is allowed, i.e. $\int_{[\alpha,\beta]} T(\theta)d\theta = 0$. This represents a slight restriction on the generality of the formulation in the presence of body forces which may be relaxed by considering non-uniformly distributed body-force potentials.

Now, the governing SIEs (46)-(47) were obtained by operating on what is one portion of the displacements in the present instance (i.e. displacements for problems I, II). Since the operator $\boldsymbol{\partial}$ is linear, the effect of the body forces in the formulation is obtained simply by applying $\boldsymbol{\partial}$ to displacements $\tilde{u}_r^{B,N}$ and $\tilde{u}_r^{B,T}$ in rotated and distributed form, and adding them to the right hand sides of the governing equations. After some algebra, one finds that the governing equations for partial-slip with body force loading of the pin are the same as Eqs. (46), (47) for center loading, except that the coefficients γ, γ' in Eq. (39) must be replaced by the slightly different coefficients γ_B, γ'_B where

$$\gamma_B = \beta^* + \frac{\alpha^*}{2} - \frac{1}{G_I} \qquad\qquad \gamma'_B = \beta^* + \frac{\alpha^*}{2} + \frac{1}{G_I} \tag{56}$$

The conditions for equilibrium Eq. (50) still apply, but the quantities P and Q must be interpreted as (known) area-resultants of the body forces, B_y and B_x. Due to the restriction discussed above, $\int_{[\alpha,\beta]} T(\theta)d\theta = 0$ is the only acceptable statement of moment equilibrium. When the pin is rigid, $G_I \to \infty$, so that $\gamma = \gamma_B$, $\gamma' = \gamma'_B$ and the two sets of equations become identical, as expected.

5 Partial Slip

The numerical method of Sundaram and Farris (2010) was used to solve the system Eqs. (46)-(51). From the point of view of applications the case of uniform body-force loading is somewhat more representative, so the results primarily consider body force loading. The differences arising due to center-force loading are highlighted where necessary.

5.1 Monotonic Loading with Body Forces or Center Load

Consider monotonically increasing, vertically directed body forces / center-loads applied to the pin. It is useful to introduce the dimensionless load parameter $L_p = (R - R_D)/(F\beta^*)$ where $F = B_y$ or P. When the parameter L_p is small, the contact is 'highly conforming'. Including β^* in L_p is particularly suitable for similar materials.

Consider a (representative) dissimilar indentation pair, Ti6Al4V-Aluminum, for which the Dundurs' mismatch parameters are $\alpha^D = -0.2503, \beta^D = -0.0594$. At low values of L_p (Fig. 3) in body force loading, the contact shear traction is a strong function of the coefficient of friction, μ, with much smaller stick-zones at lower μ. At higher values of L_p, the tractions are less sensitive to increases in μ. For instance, in the left plot in Fig. (4), the pressure traction lines are at values of μ ranging from 0 (dashed line) to some maximum value. It may be observed that the pressure traction lines at a fixed value of L_p cluster tightly when μ is varied and the differences in the tractions at a particular value of L_p brcome negligible beyond the indicated value of μ. The shear tractions show a similar trend; for instance, at $L_p = 0.5$, the shear traction changes very little when μ is increased beyond 0.4.

This 'traction saturation' phenomenon is a consequence of the fact that at higher μ, one has smaller slip zones at each stage of the loading; these smaller sizes are also attained earlier during the loading. Since energy is dissipated only in regions of relative motion (slip zones), this implies smaller incremental and overall dissipation at higher μ. As a consequence of Dundurs theorem the slip zone size is never zero, but it may be inconsequentially small. The loading may be considered *effectively* reversible.

The contact half-angle ϵ does not vary much with μ and is a rapidly decreasing function of L_p. The stick half-angle ρ, on the other hand, is more strongly dependent on μ (Fig. 5). At high values of L_p and μ, one also has $\rho \lesssim \epsilon$.

For similar materials, major trends in contact behavior are very similar to Ti6Al4V-Al (Figs. 6, 7); however the peak pressures N_{max} are higher and ϵ smaller for the same L_p and μ than Ti6Al4V-Al. The case of an indenter made of a more compliant material was also investigated (Al-Ti6Al4V); the three material pairs are compared in the left plot in Fig. 8. The Al-Ti6Al4V pair results in the highest N_{max}. This plot

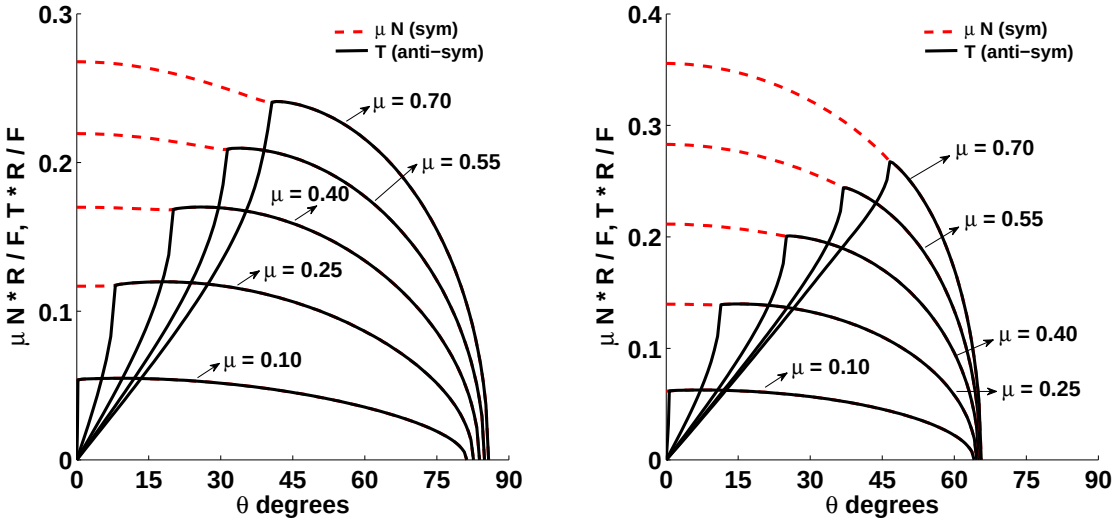

Fig. 3. Tractions in body force loading (Ti6Al4V on Al), $L_p = 0.01$ (left) and $L_p = 0.1$ (right)

also shows that at low L_p, the influenece of μ on the peak pressure is quite strong, with higher μ leading to lower peak pressures (N_{max}). For instance, the peak pressure at $\mu = 0.7$ is less than half that at $\mu = 0.1$ when $L_p = 0.01$ for Ti6Al4V-Al. For all material pairs, this influence of μ on peak pressure diminishes at higher values of L_p.

The plot on the right in Fig. 8 depicts relative magnitudes of the stick size to the contact size. In sharp contrast with half-plane contacts, where the ratio of these sizes is always 1 for similar materials, there is a strong dependence on both L_p and μ in conforming similar contacts, which is due entirely to geometric dissimilarity. Further, the fact that these relative magnitudes are functions of L_p for all indentation pairs indicates a lack of self-similarity, which is again in contrast to half-plane indentation.

Lastly, tractions obtained with body force loading are compared with those obtained with center loading in Fig. 9. While the contact size ϵ is insensitive to the change, the use of center loading usually results in higher N_{max}, while body forces result in higher T_{max} and smaller stick zones. If one considers uniform body force loads and center loads as extreme cases representing (respectively) perfectly distributed and perfectly concentrated loading, one may conclude that the contact size in conforming contacts depends more on the resultant of the loads acting on the disk than the details of their distribution over its interior. Further, one expects the behavior in more complicated loading of the disk to be bounded by these extremes.

Note that the use of even smaller L_p values ($\approx 10^{-4}$) in monotonic loading allows one to obtain limiting (neat-fit) tractions, consistent with the observations of Ciavarella et al. (2006).

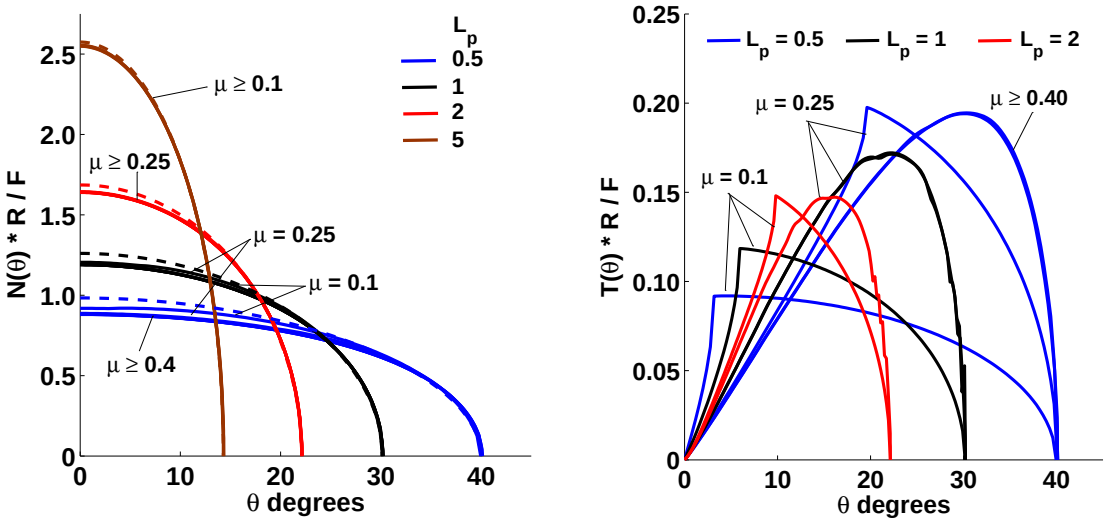

Fig. 4. Pressures (left) and shears (right) for body force loading (Ti6Al4V on Al) at high L_p at different μ. The dashed lines indicate pressures at $\mu = 0$; an increase in the values of μ beyond those indicated on the pressure plot result in negligible changes in the pressure traction.

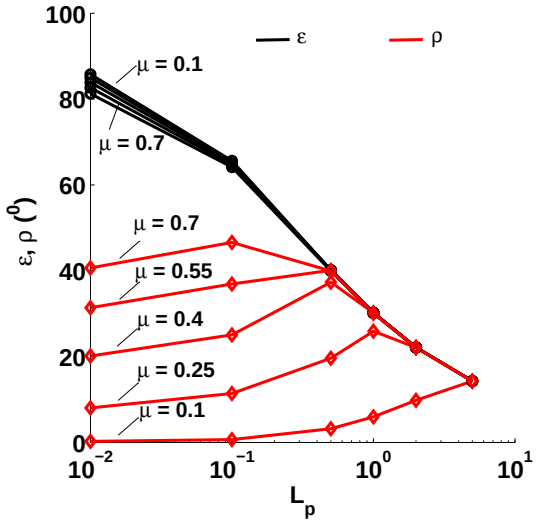

Fig. 5. Contact (ϵ) and stick-zone half-angles (ρ) for body force loading (Ti6Al4V on Al).

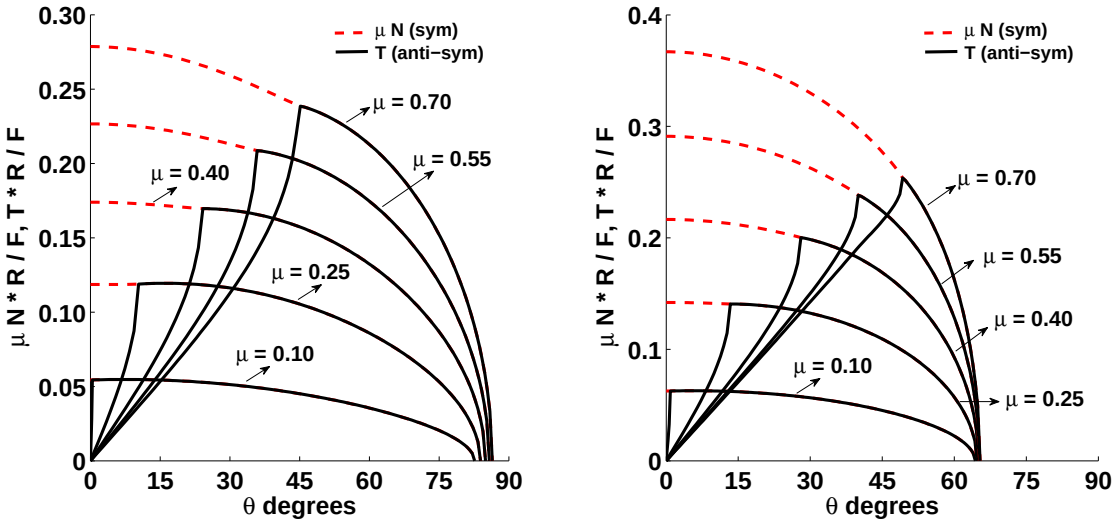

Fig. 6. Tractions in body force loading of similar materials, $L_p = 0.01$ (left) and $L_p = 0.1$ (right)

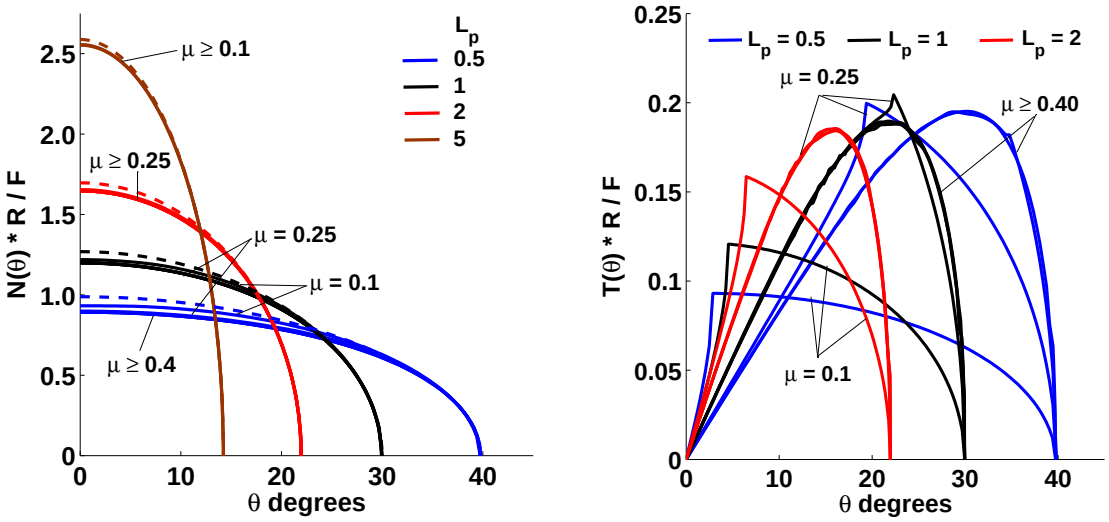

Fig. 7. Pressures (left) and shears (right) for body force loading of similar materials at high L_p at different μ. The dashed lines indicate pressures at $\mu = 0$; an increase in the values of μ beyond those indicated on the pressure plot result in negligible changes in the pressure traction.

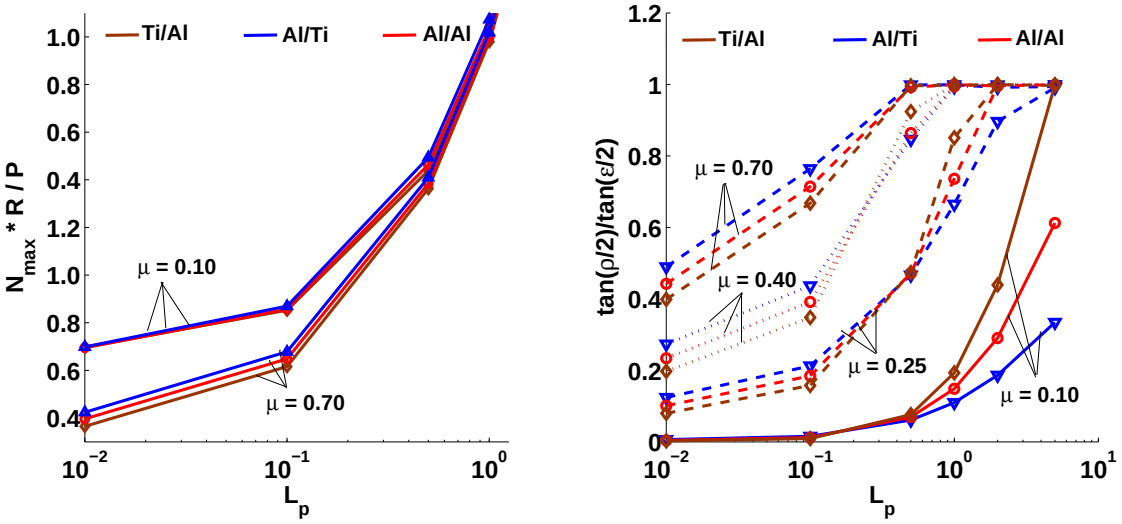

Fig. 8. Peak pressures (left) and $\frac{tan(\rho/2)}{tan(\epsilon/2)}$ (right) in body force loading.

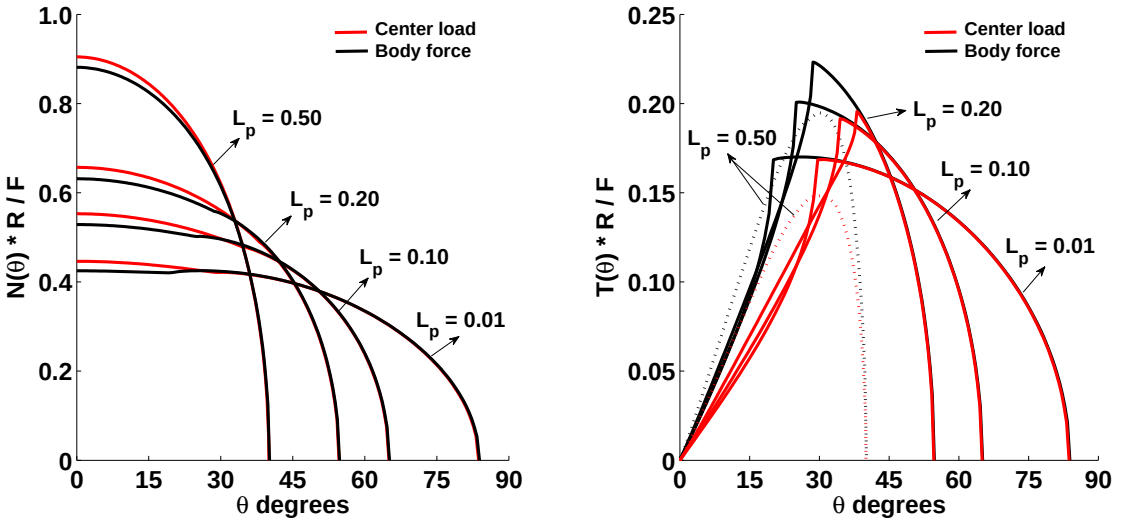

Fig. 9. A comparison of pressure(left) and shear(right) for center loading and body force loading, Ti6Al4V/Al, $\mu = 0.4$

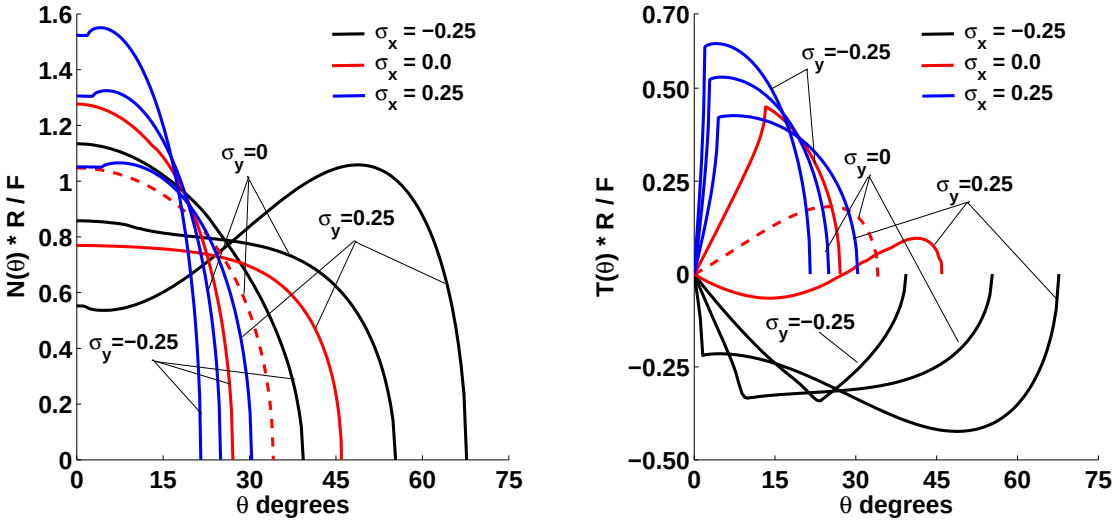

Fig. 10. Effect of remote stress on pressure (left) and shear (right) tractions with body force loading. Ti6Al4V/Al, $\mu = 0.40$, $L_p = 0.75$

5.2 Simultaneous application of body forces and remote plate stresses

Consider simultaneous application of remote stresses σ^{∞}_{xx}, σ^{∞}_{yy} to the plate accompanying body-force loading of the disk. Let normalized remote stress magnitudes σ_x, σ_y be defined as $\sigma_{x,y} = \sigma^{\infty}_{xx,yy}(R\kappa^{'})/(2GF\beta^{*})$.

The effects of remote stress application on the tractions when σ_x, σ_y are relatively low in magnitude compared to L_p (0.75) are shown in Fig. 10. The dashed lines indicate the case with zero remote stresses. The largest increase in peak pressure is observed for the case $\sigma_x = 0.25, \sigma_y = -0.25$; the largest increase in contact size occurs when $\sigma_x = -0.25, \sigma_y = 0.25$. The sign of the shear traction may flip depending on whether the remote loads aid or hinder relative tangential motion between the pin and the plate. The dramatic effect of remote stresses on contact tractions (indeed, on the very nature of the contact) is intrinsic to conforming contacts, and may be explained by the fact that the magnitude of the elastic surface displacements, $|\tilde{v}^{\infty}_r|$, may be significant compared to the gap magnitude $|h(\theta)| \approx O(R - R_D)$.

When σ_x, σ_y are relatively large compared to L_p, it is possible for the contact to become stationary (i.e. extend over 2π) or multi-part, in which case other methods of numerical solution must be sought. It may be noted that the effects of material dissimilarity and even μ are secondary in this instance.

5.3 Constrained rotation with fretting loads applied as center-loads

A typical fretting cycle consists of the application of a vertical load P in the first step, followed by cyclic variation of the horizontal load Q in subsequent steps ($+Q$, $-Q$) while keeping P constant. If the rotation of the pin is disregarded (as in half-plane fretting contacts involving cylinders), then $C_\omega = 0$. Quite different behaviors occur at low and high L_p as shown in Figs. 11 and 12; the parameter $\eta = Q/(\mu P)$. The magnitude of change in peak pressure, shift in the contact extent and difference between the peak-shear tractions on forward ($+Q$) and reversed (($-Q$) horizontal load application are significantly greater at low L_p. At higher values of L_p, the fretting tractions (qualitatively) resemble half-plane fretting tractions. However, it may be noted that due to the conforming nature of the contact, the onset of sliding (if it does occur) in the forward part of the cycle requires that $\eta_s > 1$; further, the value of η required to induce sliding in the reverse part of the cycle is usually different from η_s.

On further cycling of the horizontal loads, one finds that the tractions alternate between one of two steady-states at either extremes of the load cycle. However, in contrast to half-plane fretting contacts, the asymmetry in shape between the steady-state forward and reverse tractions persists, as seen in the left plot in Fig. 13. Further, while the shear traction in the first 'forward' step is quite different from the steady-state 'forward' shear traction, the first 'reverse' shear traction is very nearly that obtained after all subsequent load reversals. The second 'forward' traction is, however, steady-state i.e. in subsequent cycles, the tractions alternate between these two states (solid lines in the plots in Fig. 13). It is also seen (right plot in Fig. 13) that beginning the horizontal load sequence with $-Q$ instead of $+Q$, the steady-state tractions are of opposite signs, and mirror images of each other shapewise. However, the envelope of the contact arcs and the peak shear tractions are the same in both cases.

It has been suggested to us[4] that the persistent difference between the shapes of the shear tractions in the forward and reverse cycles indicates a 'system memory' effect, i.e. one in which the system retains a memory of the direction in which loading first started - a phenomenon not observed in half-plane fretting contacts.

5.4 Free rotation with fretting loads applied as body forces

Next, assume that the pin is free to rotate in response to fretting loads. This is obtained by imposing the condition $\int_{[\alpha,\beta]} T(\theta) d\theta = 0$. In this instance, let vertically

[4] by an anonymous referee

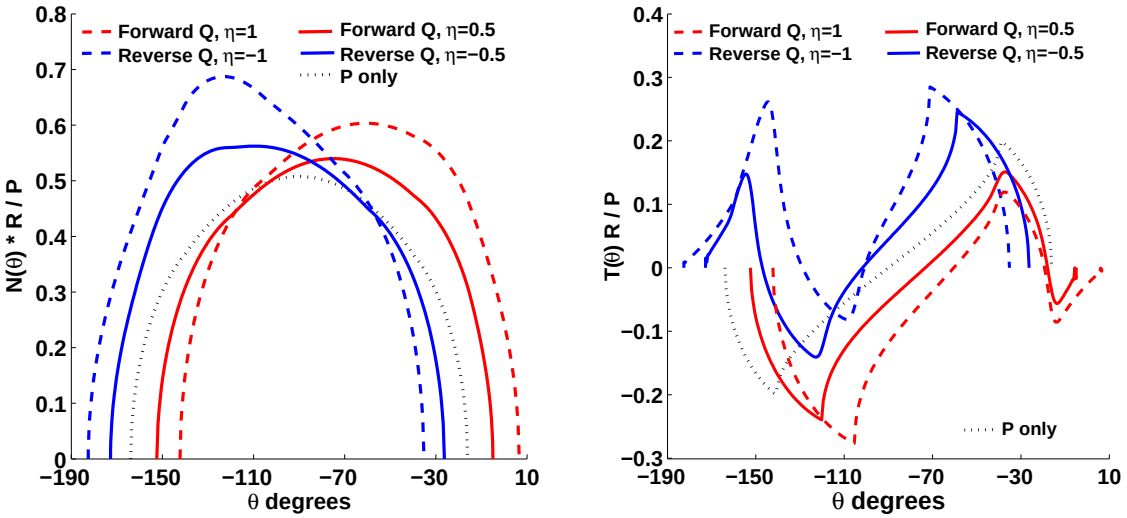

Fig. 11. Fretting type loads. $L_p = 0.05$, $\mu = 0.55$, $C_\omega = 0$, Ti/Ti

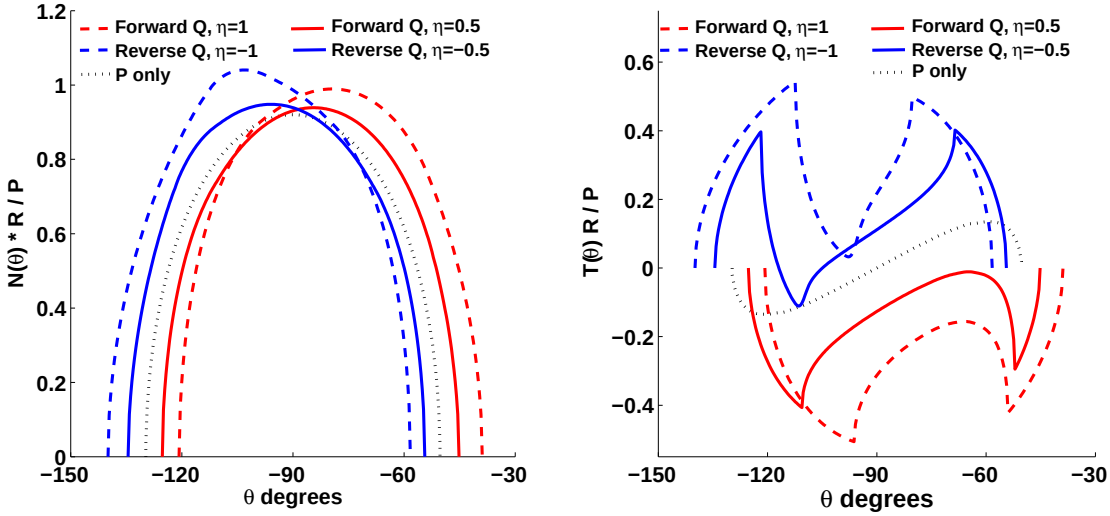

Fig. 12. Fretting type loads. $L_p = 0.50$, $\mu = 0.55$, $C_\omega = 0$, Ti/Ti.

directed body forces with resultant B_y be applied to the pin in the first step. While keeping B_y constant, horizontal body forces with resultant B_x are applied in the second step, and subsequently reversed to $-B_x$ in the third step. The rotation of the pin, $C_\omega \neq 0$ in steps two and three and is obtained as part of the solution. The parameter η is now defined as $\eta = B_x/(\mu B_y)$.

In the low L_p regime, typical tractions with 'free rotation' of the pin are shown in Fig. 14 for Ti6Al4V/Ti6Al4V indentation. While the asymmetry in peak pressures in forward and reverse horizontal loading is similar to the case with constrained rotation, with roughly similar magnitudes, the shear tractions are quite different. The peak shear tractions are of somewhat smaller magnitude in both forward and reverse loading. The magnitude of the slip zone in the direction of contact growth is very small

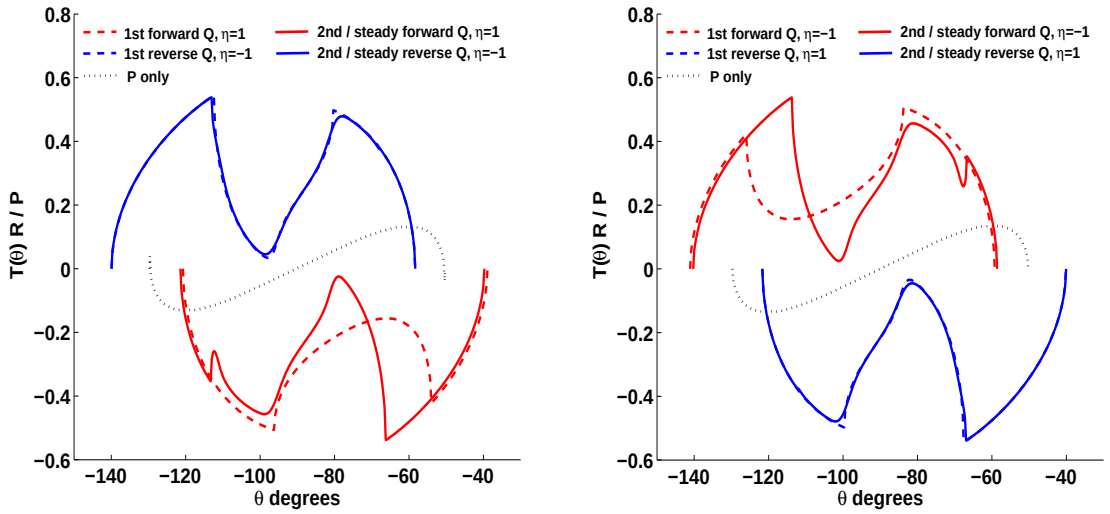

Fig. 13. Steady-state shear tractions with fretting loads. The load sequence is $0, +Q, -Q, \ldots$(left) and $0, -Q, +Q, \ldots$(right). $L_p = 0.50$, $\mu = 0.55$, $C_\omega = 0$, Ti/Ti

in both the forward and reverse cases while the slip zone on the other side is quite large. This is somewhat similar to half-plane rolling contacts. Interestingly enough, at these low values of L_p, the effect of the material properties on the tractions is not very significant. For instance, Fig. 15 shows that quite similar tractions are obtained for indentation with the use of the Ti6Al4V/Al and Al/Ti6Al4V contact pairs.

On increasing L_p (Fig. 16), the difference between the peak pressures at either end of the B_x loading cycle becomes smaller, as does the corresponding shift in the contact patch. The shear tractions are qualitatively similar to the case of $L_p = 0.05$, with higher peak shear stresses occurring at higher L_p. When L_p is increased even further, the shear peak on applying $+B_x$ is dominant; further, unlike the $C_\omega = 0$ case, the contact shift is still quite large so that the region of overlap between the contact patches in steps 2 and 3 is small, as shown in Fig. 17. Finally, it may be noted that the assumption that the pin is allowed to rotate freely generally results in less severe shears.

6 Discussion

Differences with half-plane fretting contacts

The role played by rotation in conforming fretting contacts is somewhat different than in half-plane contacts; in fretting contacts of the latter type, rotation does not enter the formulation for cylindrical profiles (unless one considers rolling contacts). It is thus not surprising that the tractions in the 'free-rotation' fretting bear a qualitative

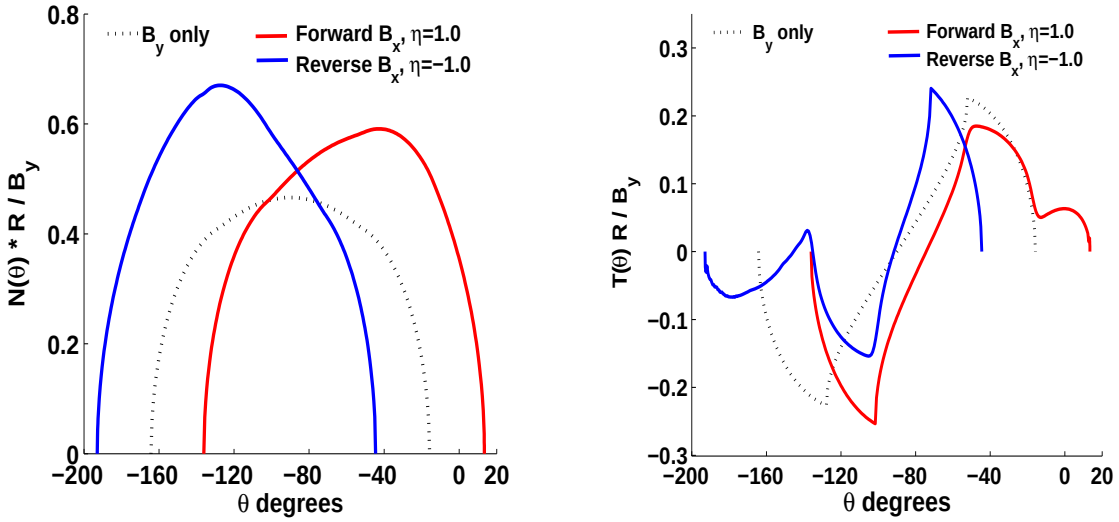

Fig. 14. Fretting type loads with body forces; the pin is free to rotate. $L_p = 0.05$, $\mu = 0.55$, Ti/Ti

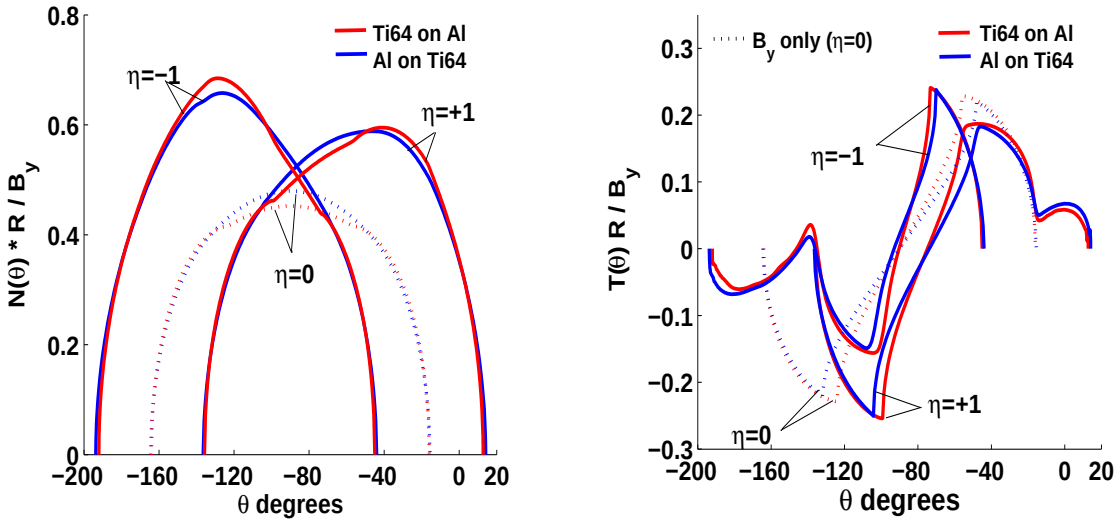

Fig. 15. Fretting type loads with body forces; the pin is free to rotate. $L_p = 0.05$, $\mu = 0.55$

resemblance to planar rolling-contacts (i.e. the shear traction in the slip zone further away from the zone of contact growth is dominant). Interestingly, while the magnitude of the pin rotation C_w in 'free rotation' is very small (ranging from 0.02 to 0.05 degrees in the test runs), the shear tractions are significantly different from the case when the pin is prevented from rotating, with the latter overestimating the severity of the shear tractions. Another point of deviation from half-plane contacts is the fact that it is harder to induce full sliding with 'fretting' loads in conforming contacts at low L_p with constrained rotation; the contacts shift and grow rather than slide, in response to higher values of η (sliding does, however, occur more easily at high values of L_p). When the pin is free to rotate, however, the onset of sliding is impossible at any L_p because the requirements $\int_{[\alpha,\beta]} T(\theta)d\theta = 0$ for free rotation and $|T(\theta)| = \mu N(\theta)$ for

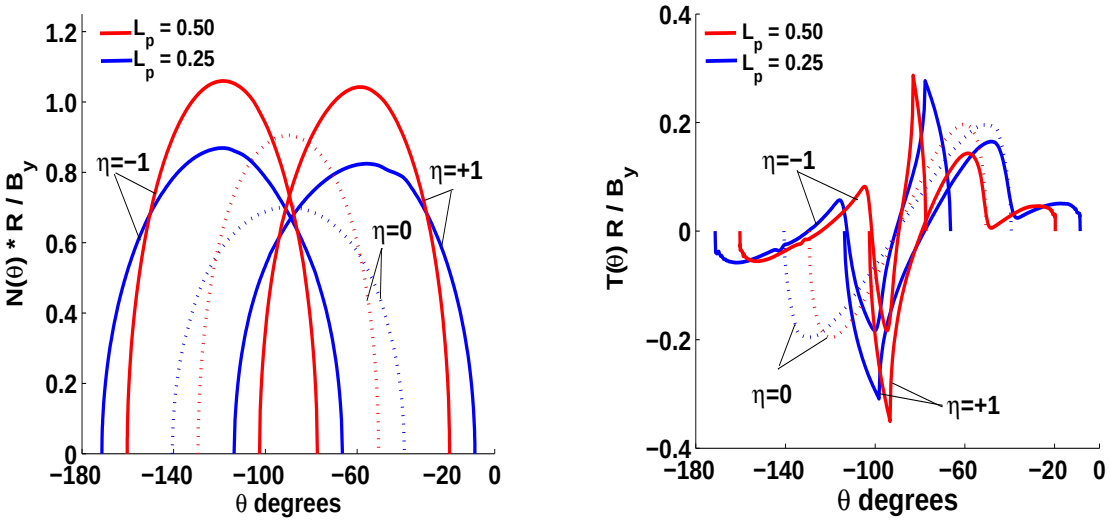

Fig. 16. Fretting type loads with body forces; the pin is free to rotate. Al/Ti6Al4V, $L_p = 0.25, 0.50$, $|\eta| = 1$

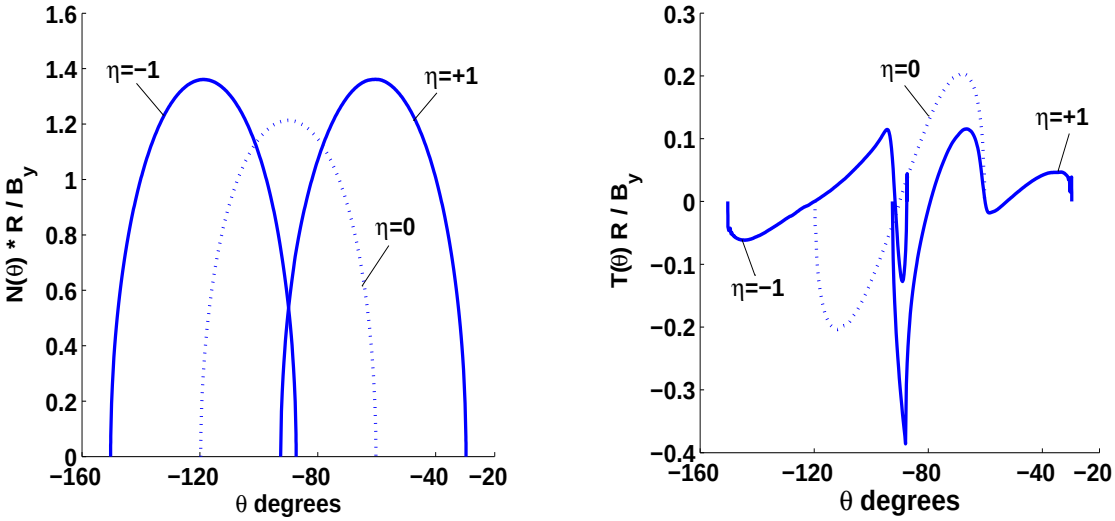

Fig. 17. Fretting type loads with body forces; the pin is free to rotate. Al/Ti6Al4V, $L_p = 1.0$, $|\eta| = 1$

full sliding are mutually exclusive at non-trivial loads. Lastly, persistent asymmetry in shape between contact shear tractions in the forward and reversed fretting cycles is another major difference between half-plane fretting contacts and conforming fretting contacts.

Sliding and frictionless indentation

By definition, $T(\theta) = \pm\mu N(\theta)$ in full sliding where μ is the coefficient of friction. Differentiating the pressure Eq. (47) with respect to θ, and subtracting the shear Eq. (46)

from it, the slip function is eliminated. This operation involves formal differentiation of principal value terms, i.e.

$$\frac{d}{d\theta}\int_{\alpha}^{\beta}\cot\left(\frac{\theta-\xi}{2}\right)N(\xi)d\xi=-\int_{\alpha}^{\beta}\frac{1}{2}\csc^2\left(\frac{\theta-\xi}{2}\right)N(\xi)d\xi \tag{57}$$

When $N(\theta)$ belongs to the class of functions H_1 with support $[\alpha,\beta]$, the integral on the right may be interpreted as a Hadamard finite-part type integral. This integral also obeys a rule for integration by parts [5] allowing it to be replaced by a Cauchy principal-value involving $N'(\theta)$. Writing $\delta^*=\gamma+\gamma'=\alpha^*+2\beta^*$, the governing Singular Integro-Differential Equation(SIDE) for full sliding with center loads is

$$\begin{aligned}R_D-R-H(\theta)=\frac{R}{4\pi}\Bigg[&\frac{\kappa'}{G}\int_{\alpha}^{\beta}N(\xi)+\delta^*\int_{\alpha}^{\beta}C(\theta,\xi)N(\xi)-\beta^*\int_{\alpha}^{\beta}\cot\left(\frac{\theta-\xi}{2}\right)N'(\xi)\\&-\pi\alpha^*N(\theta)\pm\mu\beta^*\int_{\alpha}^{\beta}\cot\left(\frac{\theta-\xi}{2}\right)N(\xi)\mp\mu\delta^*\int_{\alpha}^{\beta}S(\theta,\xi)N(\xi)\mp\mu\pi\alpha^*N'(\theta)\Bigg]\end{aligned} \tag{58}$$

where $H(\theta)=\frac{R\kappa'}{2G}\left[\mathscr{A}/2-3\mathscr{D}\cos(2\theta)\right]$ and the integrations are with respect to ξ. It is straightforward (but tedious) to show that when $\mu,\mathscr{A},\mathscr{D}=0$, this equation reduces to Persson's equation for frictionless indentation. For frictionless indentation, the condition $\int_{[\alpha,\beta]}T(\theta)d\theta=0$ is satisfied so that the same form of the SIDE also holds for pure body force loading. However, since $\delta^*=\gamma+\gamma'=\gamma_B+\gamma'_B$, one arrives at the interesting conclusion that the governing equations for frictionless center-loading and uniform body-force loading are the same and, consequently, yield the same pressures and contact extents provided these loads have the same resultants [6]. Of course, the stresses in the pin will be different. This equivalence was not obtained in earlier analyses of frictionless problems involving body forces (e.g. the 'cradling' problem in Gladwell (1980)) because algebraic simplicity dictated the choice of the form of the body force potentials there.

7 Conclusions

The SIEs governing partial-slip conforming contacts were formulated and solved numerically. In monotonic loading, the dependence of the tractions on the coefficient of friction(μ) is strongest when the contact is highly conforming. For less conforming contacts, the tractions are insensitive to an increase in the value of μ above a certain threshold. The contact size and peak pressure are only weakly dependent on the

[5] For instance see Anfinogenov and Lifanov (2001)

[6] Assuming the loads are in the regime where the physically correct solution has a single contact patch.

pin load distribution, with center loads leading to slightly higher peak pressures and lower peak shears than distributed loads. In contrast to half-plane cylinder fretting contacts, fretting behavior is quite different depending on whether or not the pin is allowed to rotate freely. If pin rotation is disallowed, the fretting tractions resemble half-plane fretting tractions in the weakly conforming regime but the contact resists sliding in the strongly conforming regime. If pin rotation is allowed, the shear traction behavior resembles planar rolling contacts in that one slip zone is dominant and the peak shear occurs at its edge. In this case, the effects of material dissimilarity in the strongly conforming regime are only secondary and the contact never goes into sliding. Further, steady-state fretting shear tractions in the forward and reversed state show persistent asymmetry in shape. Finally, the governing integro-differential equation for full sliding was derived; in the limiting (frictionless) case, center-loading and uniform body-force loading have the same governing equation, resulting in identical pressures when their resultants are equal.

Acknowledgments

This work was supported in part by DARPA through a subcontract with GE on Propulsion System Prognosis. The authors wish to thank Professor J.R. Barber for his suggestion regarding body forces.

References

Rothman, M. 1950. Isolated Force Problems in Two-Dimensional Elasticity (I). Quarterly Journal of Mechanics and Applied Mathematics, 3(3):279-296.

Muskhelishvili, N.I. 1954. Some Basic Problems of The Mathematical Theory of Elasticity. Fourth Edition. P. Noordhoff Ltd, The Netherlands.

England, A.H. 1971. Complex Variable Methods in The Theory of Elasticity. Wiley Interscience, New York.

Gladwell, G.M.L 1980. Contact Problems in The Classical Theory of Elasticity. Monographs and Textbooks on Mechanics of Solids and Fluids. Sijthoff and Noordhoff, The Netherlands.

Ho, K.C. and Chau, K.T. 1997. An infinite plane loaded by a rivet of a different material. International Journal of Solids and Structures 34(19):2477-2496.

Hou, J.P. and Hills, D.A. 2001. Contact between a pin and a plate with a hole under interference-fit and clearance-fit conditions. Proceedings of the Institution of Mechanical Engineers Part(C), 215():629-639.

Iyer, K. 2001. Solutions for contact in pinned connections. International Journal of Solids and Structures 38(2001):9133-9148.

Anfinogenov, A.Yu. Lifanov, I.K. and Lifanov, P.I. 2001. On certain one- and two- di-

mensional hypersingular integral equations. Matematicheskiĭ Sbornik 192(8):1089-1131.

Ciavarella, M. Baldini, A. Barber, J.R. and Strozzi, A. 2006. Reduced dependence on loading parameters in almost conforming contacts. International Journal of Mechanical Sciences 48(2006):917-925

To, Q.D. He, Q.-C. Cossavella, M. Morcant, K. and Panait, A. 2007. Closed-form solution for the contact Problem of reinforced pinloaded joints used in glass structures. International Journal of Solids and Structures 44(2007):3887-3903

Sundaram, N. and Farris, T.N. 2010. The generalized advancing conformal contact problem with friction, pin loads and remote loading - Case of rigid pin. International Journal of Solids and Structures 47(6):801–815.